Journal of Electron Spectroscopy and Related Phenomena 258 (2022) 147209

Contents lists available at ScienceDirect

Journal of Electron Spectroscopy and Related Phenomena

journal homepage: www.elsevier.com/locate/elspec

Non-dipole anisotropy parameters in the photoionization of Kr in the region of deep inner shell excitations

L. Ábrók [a,b,*], T. Buhr [c], Á. Kövér [a], D. Varga [a], K. Holste [c], A.A. Borovik Jr. [c], S. Schippers [c], A. Müller [d], L. Gulyás [a], S. Ricz [a,1], A. Orbán [a]

[a] Institute for Nuclear Research, H-4001, Debrecen, Hungary
[b] Doctoral School of Physics, University of Debrecen, Egyetem sqr. 1, H-4032, Debrecen, Hungary
[c] I. Physikalisches Institut, Justus-Liebig-Universität Gießen, 35392, Giessen, Germany
[d] Institut für Atom- und Molekülphysik, Justus-Liebig-Universität Giessen, D-35392, Giessen, Germany

ARTICLE INFO

Keywords:
Photoionization
Angular distribution
Dipole/non-dipole anisotropy parameters
Excitations

ABSTRACT

The photoelectron angular distribution (PAD) of the Kr $4p_{1/2}$ and $4p_{3/2}$ fine structure states was measured with linearly polarized synchrotron radiation in the vicinity of the resonant excitations of the $3p$ subshell. Experimental dipole and non-dipole anisotropy parameters were determined from the measured angular differential cross sections. In order to interpret our experimental results we have used a theoretical model going beyond the dipole approximation considering the quadrupole and octupole terms for the direct photoionization. We have taken into account several autoionization channels relevant for the studied photon energy range. The photon energy dependence of the measured anisotropy parameters puts in evidence the importance of the channel interactions. Moreover, unexpectedly large non-dipole contribution have been observed.

1. Introduction

The study of the angular distribution of electrons ejected in photoionization, besides the dynamics of the process, gives detailed information on the structure of atoms and on the role of multielectron correlation. At photon energies as low as a few hundreds eV, non-dipole contributions were supposed to be negligible [1], while at high energies (above 5 keV), a realistic description requires many multipoles to be included [2].

Experimental results due to advances in synchrotron light sources posed the question of the validity of the dipole approximation (DA) at low photon energies [3,4]. It is usual practice to ignore the non-dipole contributions for photoionization, however there are experimental indications that their inclusion might be important down to even of a few tens of eV energies [5,6]. This is especially true for angular differential cross sections. Previously, experimental observation of non-dipole effects beyond the dipole-quadrupole interference was reported in the photoionization of the Ne $2p$ valence electrons in the 800–1500 eV photon energy range [7]. Later, non-dipole contributions significantly higher than expected by theory, have been found for Kr at 60–110 eV photon energies [8] in the region where the electric quadrupole related cross section has a minimum (see Cooper minima of electric quadrupole channels [9]). Moreover, the inclusion of excitations cannot be neglected when trying to understand the experimental results of the angular differential cross sections. Calculations for angular distributions were done for the case of Xe $5s$ and $5p$ subshells from a few tens of eV to 200 eV by Johnson and Cheng with the aim of comparing various Relativistic Random-Phase Approximation (RRPA) predictions including different coupled excitation channels [10]. Their results show significant non-dipole contributions compared to the RRPA calculations without excitations and strong variations of all the anisotropy parameters as a function of the photon energy. Several experimental and theoretical studies have been published focusing on the non-dipole effects in the energy region of the Cooper minima [11] as well as on the observation of interference effects between the direct photoionization and resonant processes [12–14]. Phenomena like Cooper minima [15] or enhanced photon yield due to resonances have also been found in high harmonic generation (HHG) [16–18], indicating the breakdown of the dipole approximation at low energies. Thus, the importance of non-dipole ionization studies cannot be neglected.

Earlier investigations focusing on the $3d \rightarrow np$ and the $4d \rightarrow np$ resonant excitations in the photoionization energy dependence of the Kr $4s$ and Xe $5s$ subshells, respectively, showed that the measured dipole

* Corresponding author at: Institute for Nuclear Research, H-4001, Debrecen, Hungary.
E-mail address: abrok.levente@atomki.hu (L. Ábrók).

[1] In memoriam of our late colleague Sándor Ricz, who had the leading role in the investigation of non-dipole effects in photon–atom interaction as well as in the development of the electron spectrometer used in the present experiment.

https://doi.org/10.1016/j.elspec.2022.147209
Received 13 April 2022; Received in revised form 18 May 2022; Accepted 29 May 2022
Available online 3 June 2022

parameters could only be explained by considering the resonant excitation processes together with the direct photoionization, i.e. highlighting the role of channel interactions [12]. In our previous work [19] we have investigated, in addition to the dipole parameter, the role of the non-dipole anisotropy parameters of the Kr 4*p* photoelectron angular distributions in the photon energy range of the Kr 3*d* → n*p* resonant excitations. Qualitative agreement was found for the dipole parameters between our experiments and theoretical results [19]. Both the dipole and non-dipole parameters showed the role of interference between the direct ionization and the resonant excitation participator Auger decay process.

Based on these results in this work we focus on the influence of autoionization processes related to deeper lying excited subshells, to see the change on the observable angular distributions and on the ability of the theories. We expect that due to the different electron correlation of the inner subshell's electrons, the photoelectron angular distribution of the Kr 4*p* photoionization could be strongly different from the outer lying 3*d* case. The energy of the incident photon beam lies between 205–230 eV, where the Kr 3*p* → n*s*/m*d* resonances can be excited. In [19] we have focused on the dipole and quadrupole transitions, in the present case the photon energy range is larger than the corresponding dipole and quadrupole transitions energies. The photon beam was linearly polarized. From the measured angular distributions we determined the dipole (β) and non-dipole anisotropy parameters (γ, δ and ν) for the two fine structure components of the Kr 4*p* orbital.

The theoretical model used for the interpretation of our previous study of the 4*p* photoionization in the vicinity of the 3*d* resonant excitations gave qualitative agreement for the β parameter. Thus we use the same model to interpret our present results. Since in this case inner shell processes are involved instead of hydrogenlike wavefunctions we consider Hartree–Fock wavefunctions. Moreover, we also want to give a theoretical estimation for the non-dipole anisotropy parameters, therefore we include contributions beyond the DA for the direct ionization. Our measurement shows a strong increase of the non-dipole anisotropy parameter γ with increasing photon energy in disagreement with the existing theoretical calculations. Moreover, our experiment also shows unexpectedly large ν parameters, larger than δ and comparable to γ. The reevaluation of our previously measured data [19] leads us to the same conclusion for ν in the case of the resonant excitation of the 3*d* subshell.

Our experimental results suggest that the interchannel interactions in valence shell photoionization are important not just around threshold but also above it, approximately 200 eV in the present study, in agreement with earlier observations [20–22]. The outline of the paper is as follows: in Section 2, we briefly present our experimental setup, in Section 3, we describe the theoretical basis and present our model. In Section 4, we show and discuss our results and Section 5 contains our conclusions and an outlook. Atomic units are used throughout the paper, unless otherwise stated.

2. Experiment

The experiment was carried out at the BW3 beamline of the DORIS III synchrotron light source [23,24] at HASYLAB (Hamburg, Germany). An ESA-22D electrostatic electron spectrometer was used to analyze the emitted electrons. The detailed description of ESA-22-type electron spectrometers is available in Refs. [19,25]. The spectrometer consists of a spherical and a cylindrical mirror analyzer. The spherical mirror focuses the electrons from the scattering plane to the entrance slit of the cylindrical analyzer which performs the energy analysis of the electrons. The electrons ejected into the $\theta = 0°–360°$ polar angular range are detected simultaneously by 22 channeltrons positioned at multiples of 15°. The angular range seen by each channeltron is ±3.5°. θ and ϕ define the polar and azimuthal angles relative to the polarization vector of the photon. The interaction region is shielded with two layers of μ-metal sheets, hence the residual magnetic field is less than 5 mG.

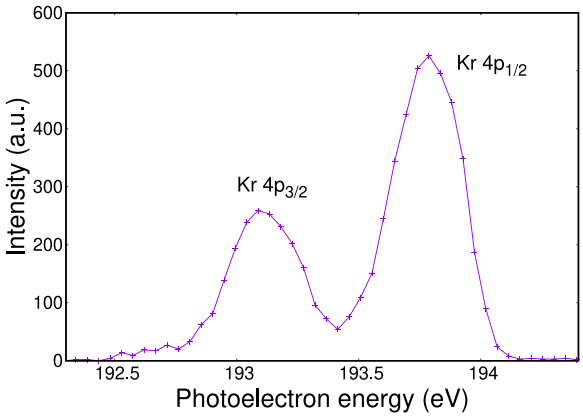

Fig. 1. Measured photoelectron spectrum of the fine structure components of krypton 4*p* vacancy (purple cross) for $\theta = 30°$ and $\phi = 0°$ at 209 eV photon energy.

The angular distribution of Kr 4*p* photoelectrons was measured at the pass energy of 50 eV resulting in about 114 meV (FWHM) energy resolution of the spectrometer. The bandwidth of the photon beam was approximately 470 meV using a width of 500 μm for the monochromator exit-slit in the 3*p* →ns/md resonant excitation range. Due to the energy resolution of the analyzer and the bandwidth of the photon beam we could separate the spin–orbit components of the Kr 4*p* photoelectron lines as illustrated in Fig. 1.

The relative efficiencies of the detectors were determined by measuring the known (dipole) angular distribution of Ne 2*s* photoelectrons ionized by 250 eV photons. The kinetic energy of the emitted electrons in case of the Ne 2*s* is within the studied energy range of the Kr 4*p* photoelectrons.

The experimental angular anisotropy parameters of the Kr 4*p* photoelectrons were obtained by fitting the efficiency-corrected experimental intensities using the following equation:

$$\frac{d\sigma_{nlj}}{d\Omega} = \frac{\sigma_0}{4\pi}\left[1 + \beta P_2(\cos\theta) + (\delta + \gamma\cos^2\theta)\sin\theta + 2\nu P_4(\cos\theta)\right] \quad (1)$$

where σ_{nlj} is the photoionization cross section of the nlj orbital, σ_0, β, γ, δ and ν are the fitting parameters (for details see Section 3.), P_2 and P_4 are the second- and fourth-order Legendre polynomials, respectively. This formula describes the angular distribution of photoelectrons ejected from a randomly oriented sample by linearly polarized light (see Section 3.).

3. Theoretical estimation

The theoretical model presented in our earlier study [19], in which the channel interaction between the direct ionization and the resonant Auger decay channels were considered, has also been applied in the present study. In the earlier work, where the valence shell photoionization of the Kr 4*p* subshell was studied in the energy region of 3*d* excitation resonances, qualitative agreement was found between experiment and theory. Here we give a brief description of the model, emphasizing the modifications used in the present study. The independent particle model for closed-shell atoms is invoked. The electron spin is not taken into account in the calculations. We considered the following processes:

$$h\nu + Kr\left([Mg]\,3p^6\,3d^{10}\,4s^2\,4p^6\right) \rightarrow Kr^+(4p)^{-1} + e^{-\,\text{direct}}_{photo}$$
$$h\nu + Kr\left([Mg]\,3p^6\,3d^{10}\,4s^2\,4p^6\right) \rightarrow Kr^*[(3p)^{-1}n_k l_k]$$
$$\rightarrow Kr^+(4p)^{-1} + e^{-\,\text{resonant}}_{p_{Auger}}$$

The first line stands for the direct photoionization process while the second one is the resonant process, showing the excited states and their

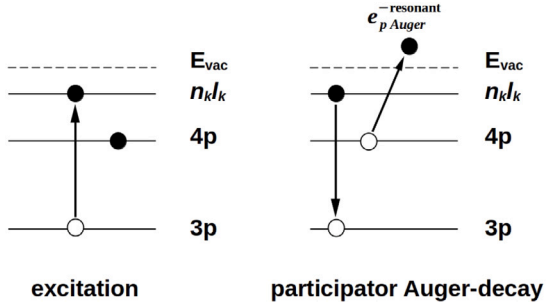

Fig. 2. A $3p$ resonant excitation and a possible participator Auger process.

Auger decay (for an example see Fig. 2). n_k is the principal quantum number of the intermediate excited state, while l_k denotes its angular momentum quantum number. We emphasize that the second process is only possible when the photon energy equals the energy difference of the initial and excited states. Interference between the direct ionization and excitation-decay pathways is possible if the kinetic energies of the emitted electrons ($e^{-\text{ direct}}_{photo}$ and $e^{-\text{ resonant}}_{p_{Auger}}$) are the same in both cases. In this model it was assumed that the resonances are discrete, with no overlap between them.

The interaction Hamiltonian for the direct process can be expanded into Taylor-series:

$$H_{int} = \sqrt{\frac{2\pi}{\omega}} exp(i\mathbf{kr})\boldsymbol{\epsilon}\mathbf{p} \sim (1 + i\mathbf{kr} + \frac{1}{2!}(i\mathbf{kr})^2 + \cdots)\,\boldsymbol{\epsilon}\mathbf{p}, \tag{2}$$

where the first term is referred to as the dipole contribution. The length form of the transition matrix elements was used throughout our calculations. Contributions up to the quadratic term were considered in the present work and the ionization matrix element takes the following form:

$$M^{dir.}_{fi} \sim i\omega\langle z\rangle + \frac{1}{2}(\alpha\omega)i^2\omega\langle xz\rangle - (\alpha\omega)^2\frac{1}{3}i\omega\langle x^2 z\rangle \tag{3}$$

where we used the notation $\langle O\rangle = \langle\psi_f|O|\psi_i\rangle$. The fine-structure constant and the photon energy are denoted as α and ω, respectively. The first term corresponds to the usual electric dipole (E1) approximation while the second and third terms can be associated with electric quadrupole (E2) and electric octupole transitions (E3). Thus, in this case the angular momentum of the outgoing partial wave is not limited to the $l-1$ and $l+1$ selection rules of the dipole transitions (l is the angular momentum quantum number of the initial state). In the case of the DA for linearly polarized light the differential cross section [26] is given by

$$\frac{d\sigma_{nlj}}{d\Omega} = \frac{\sigma_0}{4\pi}\left[1 + \beta_{DA}P_2(\cos\theta)\right]. \tag{4}$$

Here β_{DA} comes from the squared electric dipole term (E1) for the direct process.

The different electric multipole terms of Eq. (3) can interfere with each other as one can see below in the squared transition matrix element expressed as

$$\begin{aligned}|M^{dir.}_{fi}|^2 \sim\ & \overbrace{\omega^2|\langle z\rangle|^2}^{E1-E1} + \frac{1}{4}\overbrace{\alpha^2\omega^4|\langle xz\rangle|^2}^{E2-E2} + \overbrace{(\alpha\omega)^4\frac{1}{9}\omega^2|\langle x^2 z\rangle|^2}^{E3-E3} \\ & + \overbrace{\frac{1}{2}\alpha\omega^3 i\Big(\langle z\rangle^*\langle xz\rangle - \langle z\rangle\langle xz\rangle^*\Big)}^{E1-E2} \\ & + \overbrace{\frac{1}{6}\alpha^2\omega^4\Big(-\langle z\rangle\langle x^2 z\rangle^* - \langle z\rangle^*\langle x^2 z\rangle\Big)}^{E1-E3} \\ & + \overbrace{(\alpha\omega)^3\frac{1}{12}\omega^2 i\Big(\langle xz\rangle^*\langle x^2 z\rangle - \langle xz\rangle\langle x^2 z\rangle^*\Big)}^{E2-E3}.\end{aligned} \tag{5}$$

In the above expression the first three terms are the direct terms, while further ones are the interference terms between different multipoles.

In our calculation we considered the leading terms in $\alpha\omega$: $E1-E1$, $E2-E2$, $E1-E2$ and $E1-E3$ as our measurements were performed at low photon energies (at approximately 200 eV). The terms $E2-E3$ and $E3-E3$ proportional to ω^5 and ω^6 are expected to contribute significantly to the cross section only at higher photon energies and therefore, they are neglected here.

The final expression for the angular distribution beyond DA for linearly polarized light is

$$\begin{aligned}\frac{d\sigma_{nlj}}{d\Omega} = \frac{\sigma_0}{4\pi}\ & \Big[1 + \beta P_2(\cos\theta) + (\delta + \gamma\cos^2\theta)\sin\theta\cos\phi \\ & + \lambda P_2(\cos\theta)\cos 2\phi + \mu\cos 2\phi \\ & + \nu(1 + \cos 2\phi)P_4(\cos\theta)\Big],\end{aligned} \tag{6}$$

where β includes contributions from $E1-E1$, $E1-E3$ and $E2-E2$ terms. δ and γ are connected to $E1-E2$, whereas λ, μ and ν arise from $E1-E3$ and $E2-E2$. The measurements were performed in a geometry where $\phi = 0$, such that

$$\begin{aligned}\frac{d\sigma_{nlj}}{d\Omega} = \frac{\sigma_0}{4\pi}\ & \Big[1 + (\beta + \lambda)P_2(\cos\theta) + (\delta + \gamma\cos^2\theta)\sin\theta \\ & + \mu + 2\nu P_4(\cos\theta)\Big].\end{aligned} \tag{7}$$

As a result, the current experiment cannot separate λ from the β parameter, i.e., only the sum of β and λ can be determined here which we abbreviate with β. Based on our previous experimental observations [8] ν was found to be around two orders of magnitude higher than predicted by theory [27], and the values of μ were close to zero, in a wide photon energy range of 60–110 eV. Therefore in the analysis of the experimental data, the used fit function includes β, γ, δ and ν while λ (which is included in β) and μ are omitted.

In calculating transition matrix elements of Eq. (3) we used atomic bound and continuum wavefunctions obtained from the Hartree–Fock method with the frozen core approximation [28]. The bound and continuum orbitals were optimized on the same potential. The continuum wavefunctions were normalized to unit energy. The short-range phase shift and the Coulomb phase shift for the outgoing waves were also calculated. As a test of our theoretical model we calculated the cross sections and the angular anisotropy parameters for the direct photoionization of different orbitals in Kr. We have compared the results with the spin-dependent calculations performed by Derevianko and Johnson [27] and with those obtained by Cooper [29]. Our results strongly align with the spin dependent calculations performed by Derevianko with a slight energy shift, as Fig. 3 illustrates for the β and γ parameters. Similarly close agreement has been found for the other anisotropy parameters (δ, μ, ν and λ). Excellent agreement was found with the predictions made by Cooper [29] for the photon energies considered in their work.

We analyzed how the participator Auger decay process resulting in $(4p)^{-1}$ vacancies affects the anisotropy parameters of photoionization. The $3p^{-1}$ excited states can also decay via spectator Auger, Coster–Kronig and other participator Auger decay processes. In the measurement, we have focused on the electron energy range where the decay process results in the same atomic final state as the direct ionization of a $4p$ outer orbital electron. Electrons with lower energies were not detected in this experiment. Therefore, we omitted the other decay channels in our model.

It was assumed in [19] that the ejected electron associated with the excited state is a result of a two-step process: excitation of a bound electron to a higher excited state and the relaxation process through participator Auger decay:

$$M^{\text{exc.}}_{n''l'',l',n_k l_k} \sim \underbrace{\langle\epsilon l' m'|V|n_k l_k m_k\rangle}_{\text{Auger}}\underbrace{\langle n_k l_k m_k|H_{int}|n'' l'' m''\rangle}_{\text{excitation}}, \tag{8}$$

where V is the electron–electron Coulomb potential and H_{int} corresponds to the interaction of the electrons with the photon field. The

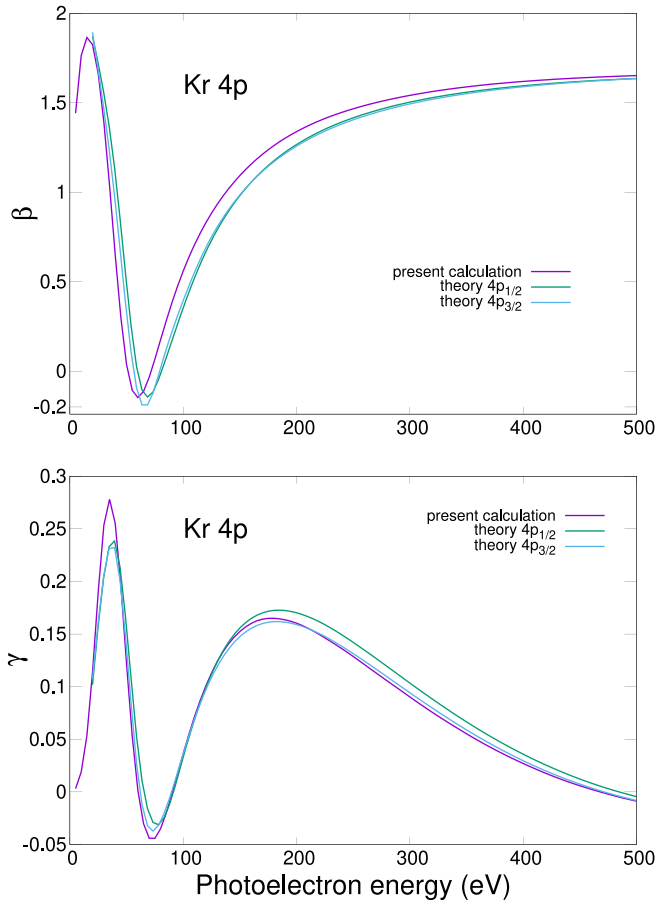

Fig. 3. Calculated β (in DA) and γ anisotropy parameters as a function of the photoelectron energy for the direct ionization of the krypton $4p$ subshell. Present calculations are shown in purple, while the spin dependent calculations of Derevianko and Johnson [27] are presented in green dashed and blue dotted–dashed lines corresponding to the ionization of the $4p_{1/2}$ and $4p_{3/2}$ orbitals, respectively.

continuum states, the intermediate states and the initial states of the Auger process are denoted in this order as $\epsilon l'm'$, $n_k l_k m_k$ and $n''l''m''$. As in our previous work [19], we included the matrix element of the excitation process in the theoretical estimation. Only dipole transitions were considered for the excitation.

The total transition matrix element is the sum of the partial matrix elements (direct ionization and excitation-autoionization processes):

$$M^{\text{dir.+exc.}} = \sum_{l'} M^{\text{dir.}}_{4pm,\,l'm'} + \sum_{l',n_k\,l_k\,m_k} M^{\text{exc.}}_{3pm'',\,n_k\,l_k\,m_k,\,l'm'}, \tag{9}$$

where the summation is performed over the continuum and intermediate states ($n_k\,l_k = 4d$, $5s$, $5d$, $6s$, $6d$, $7s$, $7d$, $8s$, $8d$ within the confines of the DA). In the case of the direct ionization we have considered electric dipole ($l' = 0, 2$), electric quadrupole ($l' = 1, 3$) and electric octupole transitions ($l' = 0, 2, 4$). From this point on, the cross section and anisotropy parameter calculations can be done in a straightforward manner. For linearly polarized light in the DA $m'' = m_k$, $m' = m$ are required to obtain identical electrons in the outgoing continuum channels for the two processes. For quadrupole transitions $m' = m \pm 1$ and for octupole transitions $m' = m$, $m \pm 2$.

Considering the electric quadrupole and octupole terms in the photon–atom interaction as well as the resonances, the final form of the angular differential cross section of the photoionization has the form:

$$\frac{d\sigma_{nlj}}{d\Omega} = \frac{\sigma_0}{4\pi}\left[1 + \beta P_2(\cos\theta) + (\delta + \gamma\cos^2\theta)\sin\theta + 2\,\nu P_4(\cos\theta)\right] \tag{10}$$

4. Results and discussion

Regarding the Kr $4p$ photoionization we performed several Ne $2s$ efficiency calibration measurements, as we explained earlier, to account for the uncertainties of the photon flux measurement, the electron transmission through the spectrometer, and the detection efficiencies of the channeltrons. For each photon energy two calibrations were used to determine the efficiency-corrected intensities for the Kr $4p$ photoionization. The anisotropy parameters shown in Figs. 4, 5, 7, 8 are the results of two measurements: we have plotted the mean values of two sets of parameters obtained by the error-weighted fitting of the efficiency-corrected intensities with the angle dependent function of Eq. (1). The measurements were performed by using 22 independent channeltrons simultaneously. During the two weeks of the measurements the signal/noise ratios of the CEMs varied, thus unfortunately for some photon energies we have larger error bars. The error bars are the standard deviations calculated from the two sets of parameters.

The measured dipole parameter β and the non-dipole parameters γ and δ are presented in Figs. 4 and 5 for the Kr $4p_{1/2}$ and Kr $4p_{3/2}$ orbitals, respectively. The observed energy dependence shows structures with peaks and dips in the ca. 211–215 eV and 218–225 eV energy ranges. We compare our measured data with the relativistic Hartree–Fock calculation performed by Derevianko and Johnson for direct photoionization [27]. The theoretically predicted anisotropy parameters of the $4p_{1/2}$ orbital, as functions of the photon energy, are shown as green dashed lines in Fig. 4, while for the $4p_{3/2}$ orbital they are represented by the blue dotted–dashed lines in Fig. 5. In the present measurement for both of the fine-structure cases, the overall behavior of the calculated β and γ parameters shows considerable deviation from the experimental observations. In the case of the δ parameter it is important to note that the values extracted from the experiments are small and their fitting errors are large, thus the comparison between theory and experiment is not sufficiently conclusive.

In comparison to our previous work [19] the identification of the different autoionization channels in the present measurement is more difficult. Due to higher photon energies more open channels are available and therefore, the observed energy dependence of the anisotropy parameters is more complex than in the case of our $3d$ studies at smaller photon energies [19]. In contrast to the $3d$ orbital, the $3p$ orbital, which is excited in the present experiment, is a more deeply bound inner orbital of Kr where the electron correlation and the reduced screening may have a larger effect on the photoionization.

In order to identify the different structures observed in our measurements the photon energies, corresponding to dipole (D) and quadrupole transitions (Q), were calculated with the relativistic Hartree–Fock method using the Cowan program [30,31]. The resulting resonance energies are shown in the bottom parts of Figs. 4 and 5. The obtained energy positions are shifted by 3.5 eV to lower energies to fit the calculated energy of the $3p - 5s$ transition with the recent experimental one [32]. The energy positions seem to correlate with some of the structures observed in the energy dependence of the anisotropy parameters: peaks and dips are visible near the D and Q transition energies for the β and γ parameters, more remarkably for the 1/2 spin component. This might be the case for δ as well, but it is not convincing due to the large errors in this case. The comparison of the measured fine-structure parameters $\beta_{1/2}$ to $\beta_{3/2}$, $\gamma_{1/2}$ to $\gamma_{3/2}$ and $\delta_{1/2}$ to $\delta_{3/2}$ puts in evidence that the spin–orbit interaction has a noticeable effect on the resonance behavior, in contrast to the weak effect resulting from the spin-dependent calculations carried out by Derevianko and Johnson [27]. One of the most interesting features is the strong energy dependence of the γ parameter: Both fine-structure components show an increase from around 0.1 to 0.5 in the 205–230 eV photon energy range. The observed trend is in contrast with theoretical predictions [9, 27], which find a constant value around 0.15 for the γ-parameters, near the local maximum at about 200 eV (see Fig. 3). Although the beta parameter dominates the main features of the PADs, the gamma and

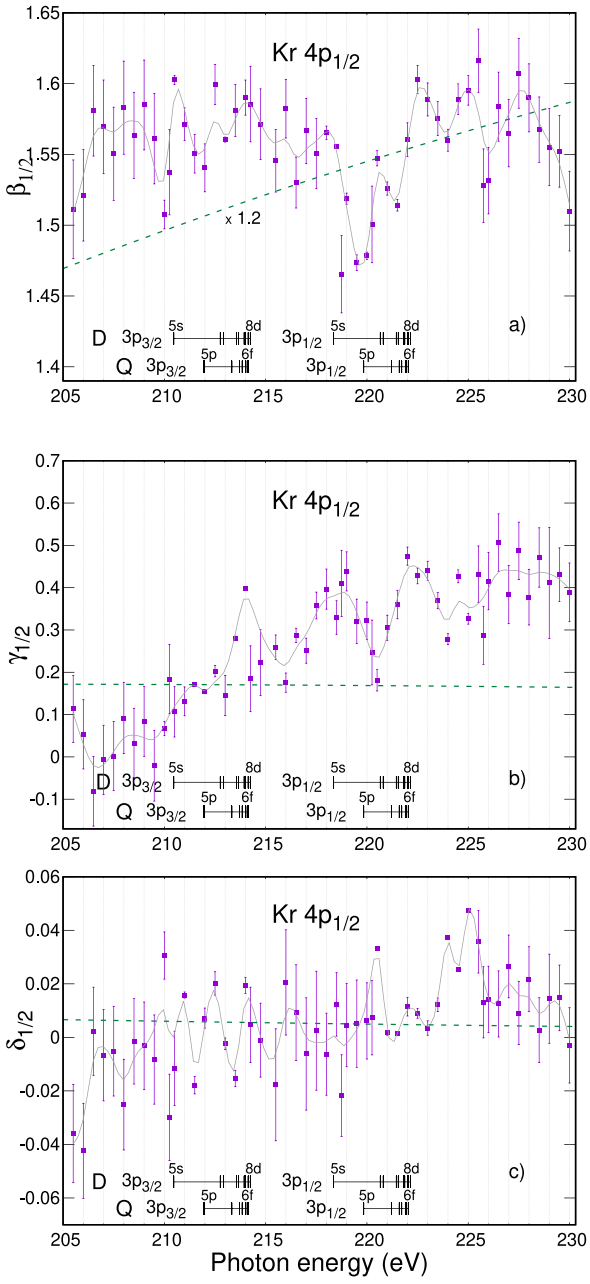

Fig. 4. The anisotropy parameter β, γ and δ (purple squares) extracted from the experiment for the Kr $4p_{1/2}$ photoelectrons in the photon energy range corresponding to the resonant excitations from the $3p$ orbital. The solid gray lines are error weighted splines to guide the eye. The vertical black bars show the energy positions of the dipole (D) transitions to $5s$, $4d$, $6s$, $5d$, $7s$, $6d$, $8s$, $7d$, $9s$, $8d$ and for the quadrupole (Q) transitions to $5p$, $6p$, $4f$, $7p$, $5f$, $8p$, $6f$, calculated with the relativistic Hartree–Fock method [30]. The green dashed lines represent the results of the spin-dependent calculations for direct photoionization only, obtained by Derevianko and Johnson [27], multiplied by 1.2 in the case of Fig. 4a.

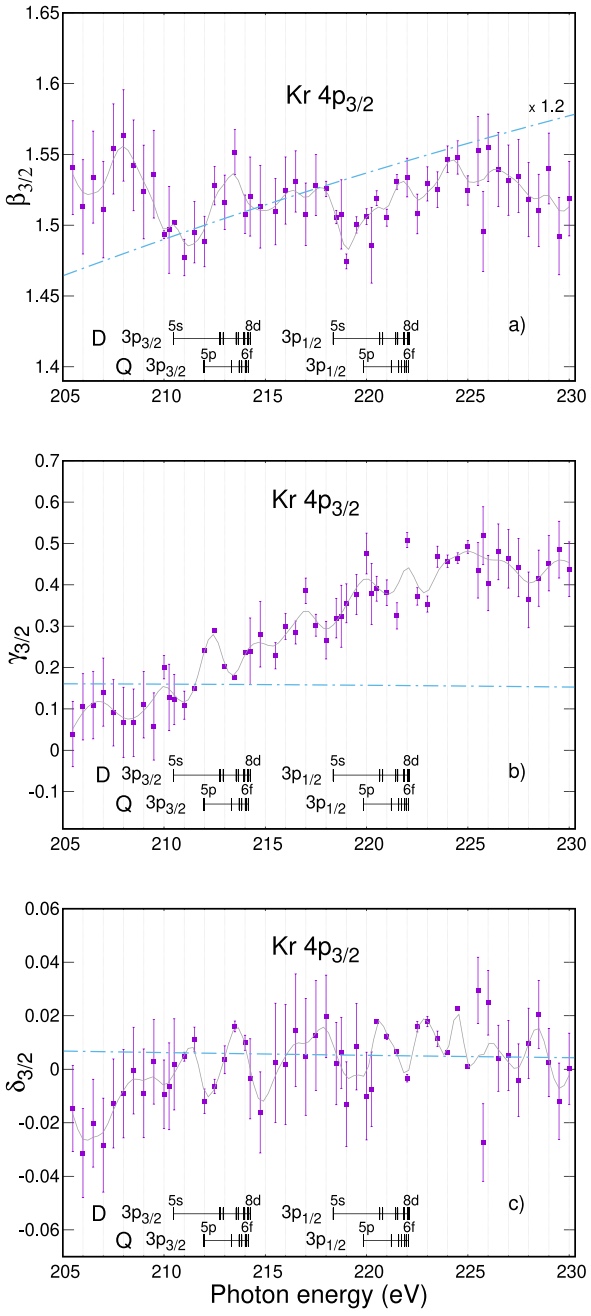

Fig. 5. The same as Fig. 4., but for the $4p_{3/2}$ photoelectrons. The blue dotted–dashed lines represent the results of the spin-dependent calculations for direct photoionization only, obtained by Derevianko and Johnson [27] multiplied by 1.2 in the case of Fig. 5a.

the delta parameters cause forward–backward asymmetry, which can be observed in the experiments. To illustrate the effects beyond the DA on the PADs, we estimated the relative difference of the angular-dependent cross section Eq. (1) for forward and backward emissions. We chose an average value for $\beta = 1.5$, and we have considered 0.1 and 0.5 for γ according to the low energy and high energy part of the energy dependence (see Fig. 5). For $\gamma = 0.1$ the relative difference between the values of the cross sections at forward angle $\theta = 30°$ and backward angle $\theta = -30°$ is 4%, while for $\gamma = 0.5$ this difference is 21%. Since the anisotropy parameter δ is smaller by an order of magnitude than the γ values, and since ν cannot introduce forward–backward asymmetry, we assumed $\delta = 0$ and $\nu = 0$ for the present estimate. Considering the role of the autoionization channels our simple theoretical model is able to predict channel interaction effects in the photoionization energy dependence of the angular parameters (see Fig. 6). The calculated parameters for the discrete resonances were convoluted

with a FWHM = 470 meV Lorentz function to account for the lifetime broadening along with the photon-energy bandwidth used in the experiment, which has a larger effect than the instrumental energy resolution. In Fig. 6a we compare our calculated β parameter with the spin-dependent calculations of [27]. One can observe that our calculations for direct ionization give larger β values, and are closer

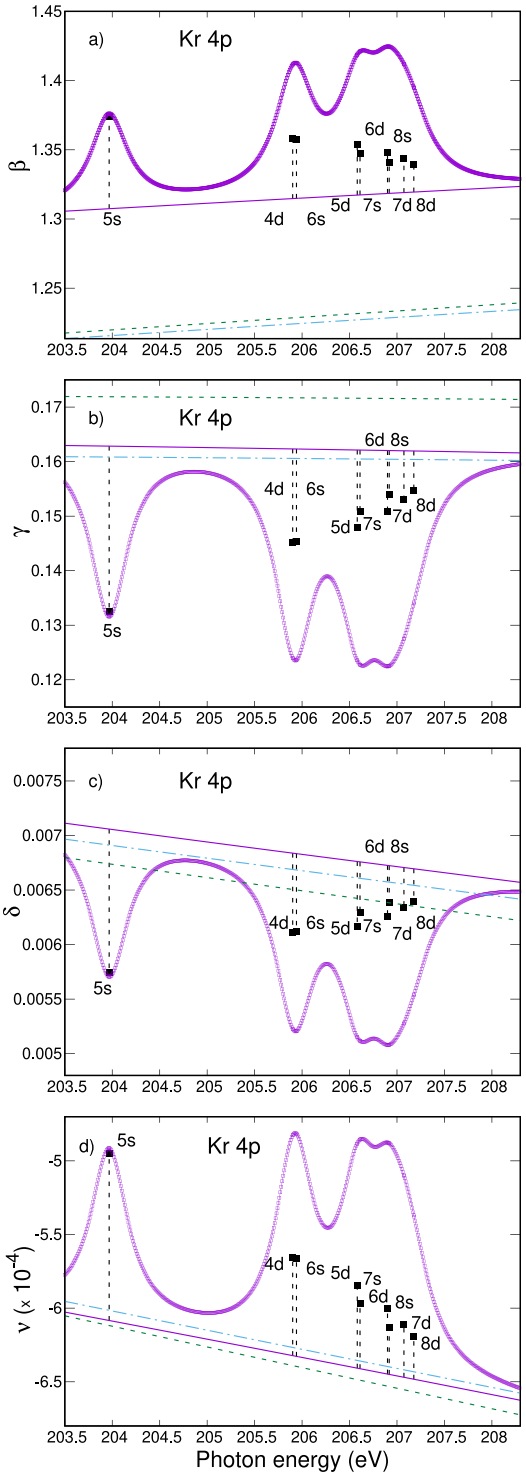

Fig. 6. Calculated anisotropy parameters β, γ, δ and ν for the Kr $4p$ photoelectrons in the photon energy range of the $3p \rightarrow n s/md$ resonant excited states: direct ionization (purple line) and ionization with the considered resonant processes (purple line with open squares). The discrete values (black squares) were calculated from the total transition matrix element Eq. (9). Their energy positions were obtained by HF-calculations [28]. Green dashed and blue dotted–dashed lines represent the spin-dependent calculations for direct photoionization obtained by Derevianko and Johnson [27] for the Kr $4p_{1/2}$ and $4p_{3/2}$ photoelectrons, respectively.

to the experimental results than the calculations by Derevianko and Johnson [27] (see Figs. 4a and 5a).

An additional prediction of our model is that for the non-dipole parameters the ratios of the resonance structures to the direct ionization are higher than in the case of β. Note that even without resonances, non-dipole parameters originate from the interference of different transition terms (e.g. E1-E2, E1-E3). Thus, they can be more sensitive to the phase differences among these various channels compared to the DA which is limited to the $l-1$ and $l+1$ channels due to the dipole selection rules. Since we do not consider all possible open channels, we cannot account for all the structures in the experimental data. For example, quadrupole excitations lead to higher bound p and f states and more partial waves l' for the outgoing photoelectrons are allowed [19]. The presence of peaks and dips in the experimental data (see Figs. 4 and 5) are not controversial with our theoretical findings, which appear to suggest either peaks only (as for β and ν) or dips only (for γ and δ) for a given anisotropy parameter: In our calculation we included autoionization channels on the basis of a simplified model [19], in which the matrix elements related to the electron–electron interaction, including phases and the fine-structure states of Kr $3p$ and $4p$ were neglected. The consequence of the insufficient treatment of the phases for the electron emission might lead to this exclusivity of obtaining just peaks or just dips for a certain anisotropy parameter. As we mentioned previously, our calculated anisotropy parameters predict similar photon energy dependences for the direct ionization as other calculations [27] (see Figs. 3 and 6), with a slight energy shift. The differences originate from the inclusion of the spin–orbit interaction [27] and electron correlation applied in the RRPA [9] which are lacking in the present treatment. Our spin-resolved experimental anisotropy parameters show quantitative and qualitative differences compared to the available theoretical calculations. Neither the previous calculations, nor the present model predict the observed behavior. The discrepancy between the experiment and the various theoretical models may be interpreted as a result of neglecting e.g. the quadrupole transitions in the resonant excitation channels [33].

In the evaluation procedure of our experimental data and in our calculations we have considered the non-dipole P_4 term of Eq. (1). Our calculations suggest that the related ν parameter is less important compared to the δ parameter, being smaller by at least one order of magnitude (see Fig. 6 c,d). The calculated ν values are in quantitative agreement with the calculation of [27], and they are much smaller than the measured ones (see Figs. 7b and 8b).

We also reevaluated our previous data related to the $3d$-subshell resonances [19] with respect to the parameter ν. The corresponding results are presented in Figs. 7a and 8a for the two fine-structure components $4p_{1/2}$ and $4p_{3/2}$. The discrepancy between theory and experiment is even larger by approximately a factor of a few hundreds. In the case of the $3d$ study, the energy width of the photon beam was much smaller than in the present experiment (approximately 20 instead of approximately 470 meV). Thus, the different structures observed in the dipole and non-dipole parameters could be assigned to certain resonant processes more easily in the experiment covering the $3d$ excitation range.

Both our current $3p$- and previous $3d$-related measurements show strong deviations from the predictions of the theoretical calculations, for all of the anisotropy parameters. Further theoretical studies of the angular distributions are needed to verify and understand these experimental observations. These findings also support the significance of detailed angular distribution measurements to extract non-dipole parameters from experiments.

The various anisotropy parameters describing the angular distributions can vary sharply with the photon energy. To emphasize the variations observed here, we compared the experimental PADs for different photon energies in Fig. 9 in the vicinity of $3d$ excitation resonances and in Fig. 10 in the region of $3p$ resonances. To normalize the data each PAD is divided by the fitted total cross section (σ_0) obtained from the measurement. In this way we have excluded the differences between the measurements at different photon energies in

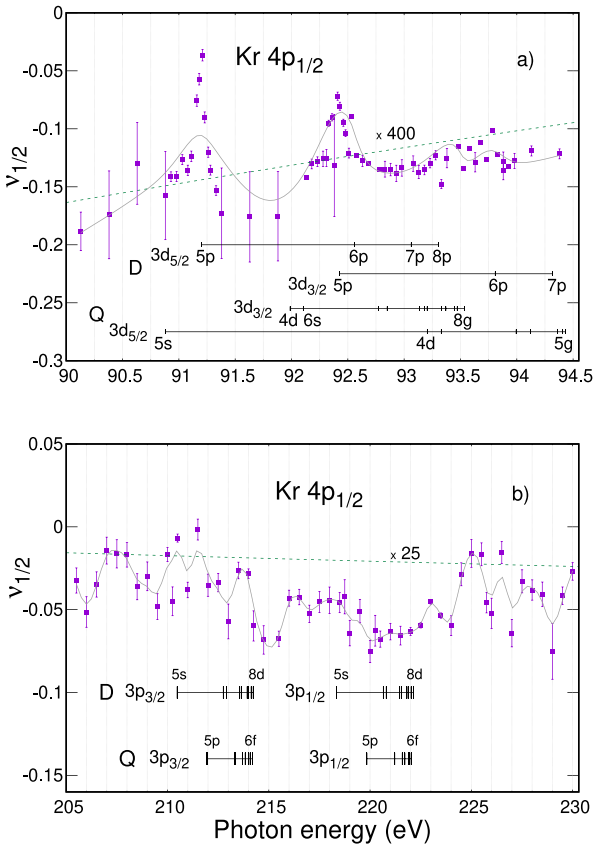

Fig. 7. The anisotropy parameter ν (purple square) extracted from the experiment for the Kr $4p_{1/2}$ photoelectrons in the photon energy range corresponding to the resonant excitations from the $3d$ (a) [19] and $3p$ (b) orbitals. The solid gray lines are error weighted splines to guide the eye. The energy positions on the black horizontal lines of 7a are taken from [19]. For 7b see the figure caption of Fig. 4. Green dashed lines represent the results of spin-dependent calculations for direct photoionization only, obtained by Derevianko and Johnson [27], multiplied by 400 and 25 in Fig. 7a and b, respectively.

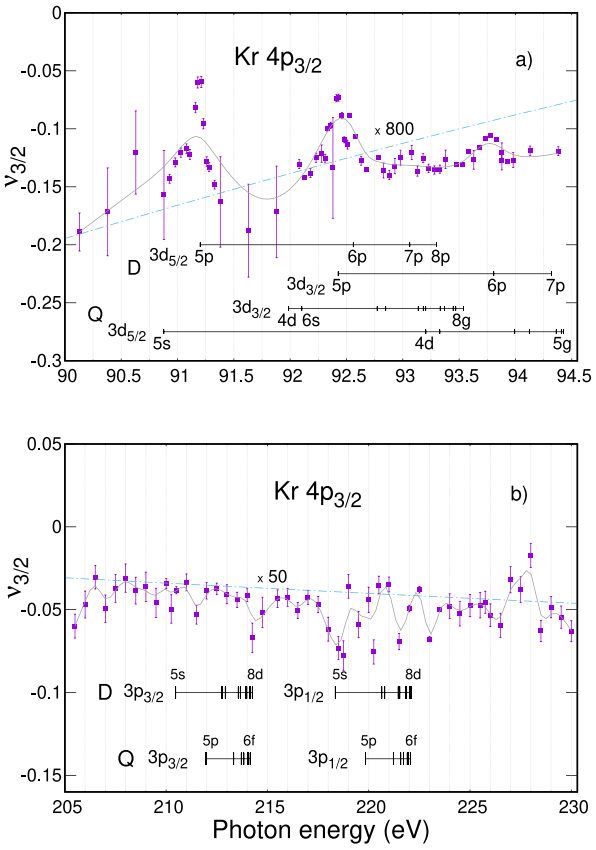

Fig. 8. The same as Fig. 7., but for the $4p_{3/2}$ photoelectrons. The blue dotted–dashed lines represent the results of the spin-dependent calculations for the direct photoionization only, obtained by Derevianko and Johnson [27], multiplied by 800 and 50 in Fig. 8a and b, respectively.

order to focus on the comparison of the angular distributions. In the case of the Kr $3d$ excitations we observe a drastic enhancement of intensities towards the angular ranges around 0° and 180° at one of the resonance energies (orange color) compared to non-resonant energies (blue and green colors). Although the shape is mostly influenced by the β parameter, other features like forward–backward asymmetry, 90°–270°, are present, which is the result of the non-dipole parameters. For the Kr $3p$ resonant excitation around 220 eV, where we see the strongest structure in the experimental $\beta_{1/2}$ parameter, (see Fig. 4a), the PAD (orange color) does not differ strongly from the PADs obtained at non-resonant energies (green and blue colors). The reason for this is that the $\beta_{1/2}$ parameter, which dominates the features of PADS, does not vary much in the studied energy range. The experimental dipole and non-dipole anisotropy parameters corresponding to Figs. 9 and 10 can be found in Tables 1 and 2, respectively.

We analyzed the effect of the different multipole contributions on the angular distributions of the photoelectrons by fitting the experimental data according to DA, Eq. (4), and considering non-dipole terms with resonances, Eq. (10), respectively. The dipole and non-dipole contributions on the PADs at photon energies 90.93 eV (for the $3d$ case) and 219 eV (for the $3p$ case) are presented in Figs. 11 and 12, respectively. In both cases we observe a noticeable γ contribution and we can observe the asymmetry introduced by the non-dipole terms in the forward–backward direction for both theory and experiment, especially for the $3d$ case in Fig. 11.

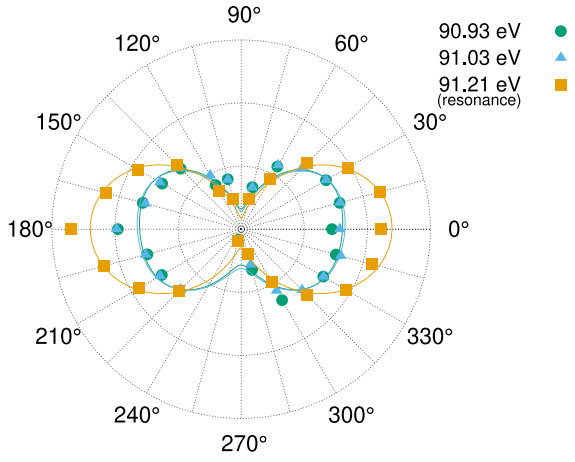

Fig. 9. Normalized angular distributions of Kr $4p_{1/2}$ for different photon energies (symbols) and the fit functions (solid lines) in the vicinity of a Kr $3d$ resonance.

5. Conclusions

With this unique experimental setup we were able to determine for the first time the photon energy dependence of the dipole (β) and non-dipole (γ, δ and ν) angular anisotropy parameters for the two fine structure components of the Kr $4p$ state with the method of angle-resolved electron spectroscopy in the photon energy range of the $3p \rightarrow ns/md$ resonant excitations. We have developed a theoretical method to interpret the experimental results by considering the channel

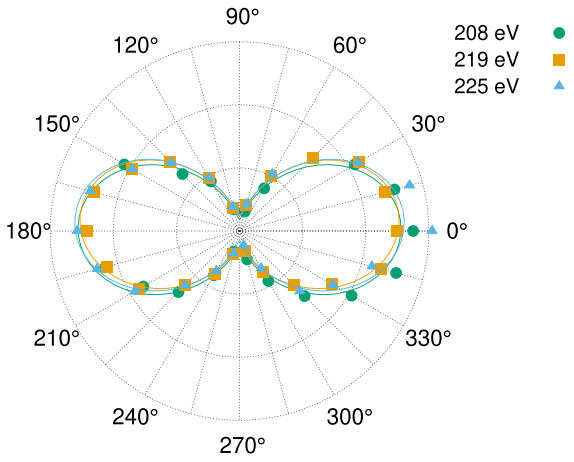

Fig. 10. Normalized angular distributions of Kr $4p_{1/2}$ for different photon energies (symbols) and the fit functions (solid lines), in the energy range of Kr $3p$ resonances.

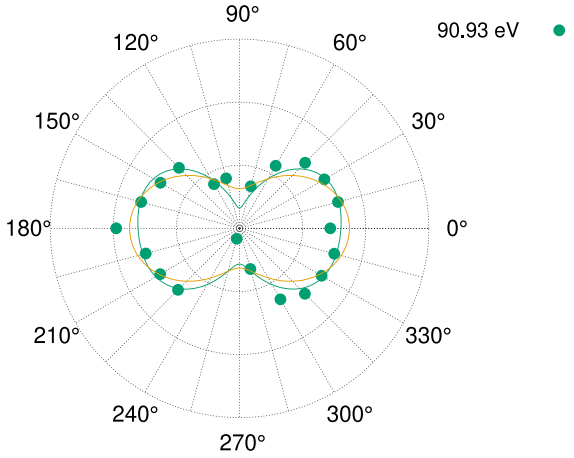

Fig. 11. Normalized angular distribution (green dot) and fits according to Eq. (4) with $\beta_{DA} = 0.743$ (orange line) and considering non-dipole terms (Eq. (10)) with $\beta = 0.904$, $\gamma = 0.210$, $\delta = -0.124$ and $\nu = -0.141$ (green line), at a fixed photon energy of 90.93 eV in the vicinity of a Kr $3d$ resonant excited state.

Table 1
Anisotropy parameters obtained by fitting the experimental data shown in Fig. 9 in the vicinity of a Kr $3d$ resonance.

Photon energy (eV)	β	γ	δ	ν
90.93	0.904 ± 0.006	0.210 ± 0.01	−0.124 ± 0.001	−0.141 ± 0.004
91.03	0.911 ± 0.005	0.264 ± 0.01	−0.175 ± 0.001	−0.126 ± 0.004
91.21	1.483 ± 0.008	0.086 ± 0.015	−0.063 ± 10^{-4}	−0.036 ± 0.005

Table 2
Anisotropy parameters obtained by fitting the experimental data shown in Fig. 10 in the photon energy range of Kr $3p$ resonances.

Photon energy (eV)	β	γ	δ	ν
208	1.559 ± 0.049	0.151 ± 0.139	−0.037 ± 0.031	−0.023 ± 0.065
219	1.516 ± 0.027	0.471 ± 0.077	−0.006 ± 0.017	−0.117 ± 0.036
225	1.602 ± 0.046	0.335 ± 0.141	0.047 ± 0.029	−0.044 ± 0.069

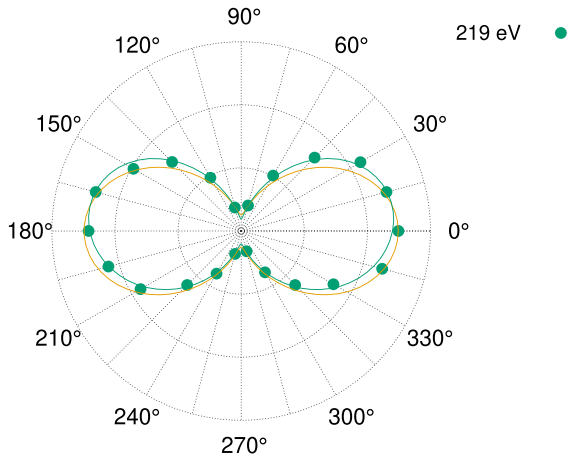

Fig. 12. Normalized angular distribution (green dot) and fits according to Eq. (4) with $\beta_{DA} = 1.49$ (orange line) and considering non-dipole terms (Eq. (10)) with $\beta = 1.516$, $\gamma = 0.471$, $\delta = 0.006$ and $\nu = -0.117$ (green line), at a fixed photon energy of 219 eV in the energy range of the Kr $3p$ resonant excited states.

interaction effects between direct ionization and autoionization. The measured anisotropy parameters, within the accuracy of the measurement, show different behavior as a function of the photon energy than the existing theoretical models predict, including the present calculation. Experimental observations show much stronger octupole contribution, ν anisotropy parameter, than predicted by theories. Our theoretical calculations considering dipole transitions are not able to give any further insight on the observed not well resolved structures. We even calculated the energy positions resulting from quadrupole transitions, but the understanding remained without success in this respect. The disagreement between the experimental anisotropy parameters for the fine structure components of the Kr $4p$ state and the values obtained from our calculations show the importance of multielectron correlation effects in photoionization. The disagreement highlights that present theories are not capable to treat these effects properly. The discrepancy observed between the experimental observations and the RRPA calculations of Banerjee et al. [9] might be due to the fact that resonant excitation processes were neglected in the calculations. The RRPA study of Johnson and Cheng pointed out the importance of excitation channels in case of the Xe 5s and 5p photoionization even tens of eV away from the subshell thresholds [10]. Another possible reason for different structures observed in the experiment may be due to the presence of multiple excitations: The two-electron excitation of the $3d$ subshell lies in the photon energy range studied here as shown in [30,31], thus using two-electron wave functions might shed additional light on some of the features observed.

Our calculations show resonance structures for all of the considered anisotropy parameters. Although these results cannot account for all the structures observed in the experiments, they give a qualitative evidence of channel interaction effects. We have also seen that the forward–backward asymmetry of the PADs is the result of non-dipole anisotropy parameters. The PADs are very sensitive to changes in the anisotropy parameters, thus future experiments with good angular resolution are needed to obtain more accurate values. By comparing experiments with different theoretical approximations we can find key points for possible refinements. More complex models are needed in which the various electron correlation effects are properly included. These findings indicate that our current understanding is still far from being satisfactory. We are currently upgrading our spectrometer by installing a position sensitive detector which will provide us a more detailed measurement of the angular distribution of the photoelectrons.

Declaration of competing interest

The authors declare that they have no known competing financial interests or personal relationships that could have appeared to influence the work reported in this paper.

Acknowledgments

We are grateful for the enlightening discussions with László Sarkadi. This work was supported by the Hungarian Scientific Research Fund (Grant No. K128621) and the National Research, Development and Innovation Office, Hungary (Grant No. 2018-1.2.1-NKP-2018-00010).

References

[1] H.A. Bethe, E.E. Salpeter, Quantum Mechanics of One- and Two-Electron Atoms, Springer-Verlag, Berlin, 1957, p. 248ff.
[2] H.K. Tseng, R.H. Pratt, S. Yu, A. Ron, Photoelectron angular distributions, Phys. Rev. A 17 (1978) 1061.
[3] O. Hemmers, R. Guillemin, D.W. Lindle, Nondipole effects in soft X-ray photoemission, Radiat. Phys. Chem. Rev. 70 (2004) 123.
[4] S. Ricz, R. Sankari, A. Kövér, M. Jurvansuu, D. Varga, J. Nikkinen, T. Ricsóka, H. Aksela, S. Aksela, Strong nondipole effect created by multielectron correlation in $5s$ photoionization of xenon, Phys. Rev. A 67 (2003) 012712.
[5] N.L.S. Martin, D.B. Thompson, R.P. Bauman, C.D. Caldwell, M.O. Krause, S.P. Frigo, M. Wilson, Electric-dipole–quadrupole interference of overlapping autoionizing levels in photoelectron energy spectra, Phys. Rev. Lett. 81 (1998) 1199.
[6] B. Krässig, M. Jung, D.S. Gemmell, E.P. Kanter, T. LeBrun, S.H. Southworth, L. Young, Nondipolar asymmetries of photoelectron angular distributions, Phys. Rev. Lett. 75 (1995) 4736.
[7] A. Derevianko, O. Hemmers, S. Oblad, P. Glans, H. Wang, S.B. Whitfield, R. Wehlitz, I.A. Sellin, W.R. Johnson, D.W. Lindle, Electric-octupole and pure-electric-quadrupole effects in soft-X-ray photoemission, Phys. Rev. Lett. 84 (2000) 2116.
[8] K. Holste, A.B. Jr., T. Buhr, S. Ricz, A. Kövér, D. Bernhardt, S. Schippers, D.V.A. Müller, Electric octupole contribution to the angular distribution of the krypton $4p$ photoelectrons, J. Phys.: Conf. Ser. 488 (2014) 022041.
[9] T. Banerjee, P.C. Deshmukh, S.T. Manson, Krypton E2 photoionization cross-section and angular distribution of photoelectrons, J. Phys. Conf. Ser. 80 (2007) 012001.
[10] W.R. Johnson, K.T. Cheng, Strong nondipole effects in low-energy photoionization of the $5s$ and $5p$ subshells of xenon, Phys. Rev. A 63 (2001) 022504.
[11] G.B. Pradhan, J. Jose, P.C. Deshmukh, L.A. LaJohn, R.H. Pratt, S.T. Manson, Cooper minima: a window on nondipole photoionization at low energy, J. Phys. B 44 (2011) 201001.
[12] S.B. Whitfield, R. Wehlitz, H.R. Varma, T. Banerjee, P.C. Deshmukh, S.T. Manson, Resonance-induced deviations of β from 2.0 for rare gas s-subshell photoionization, J. Phys. B 39 (2006) L335.
[13] S. Ricz, J. Nikkinen, R. Sankari, T. Ricsóka, A. Kövér, D. Varga, S. Fritzsche, H. Aksela, S. Aksela, Interference effects in the angular distribution of Ar $3p$ photoelectrons across the $2p \rightarrow ns/md$ resonances, Phys. Rev. A 72 (2005) 014701.
[14] T.W. Gorczyca, F. Robicheaux, Auger decay of the photoexcited $2p^{-1}$nl Rydberg series in argon, Phys. Rev. A 60 (1999) 1216.
[15] A.D. Shiner, B.E. Schmidt, C. Trallero-Herrero, P.B. Corkum, J.-C. Kieffer, F. Légaré, D.M. Villeneuve, Observation of Cooper minimum in krypton using high harmonic spectroscopy, J. Phys. B 45 (2012) 074010.
[16] J. Rothhardt, S. Hädrich, S. Demmler, M. Krebs, S. Fritzsche, J. Limpert, A. Tünnermann, Enhancing the macroscopic yield of narrow-band high-order harmonic generation by Fano resonances, Phys. Rev. Lett. 112 (2014) 233002.
[17] E.S. Toma, P. Antoine, A. de Bohan, H.G. Muller, Resonance-enhanced high-harmonic generation, J. Phys. B 32 (1999) 5843.
[18] M.A. Fareed, V.V. Strelkov, N. Thirè, S. Mondal, B.E. Schmidt, F. Légaré, T. Ozaki, High-order harmonic generation from the dressed autoionizing states, Nature Commun. 8 (2017) 16061.
[19] S. Ricz, T. Ricsóka, K. Holste, A.B. Jr., D. Bernhardt, S. Schippers, A. Kövér, D. Varga, A. Müller, Interference effect in the dipole and nondipole anisotropy parameters of the kr $4p$ photoelectrons in the vicinity of the kr $(3d)^{-1} \rightarrow np$ resonant excitations, Phys. Rev. A 81 (2010) 043416.
[20] O. Hemmers, R. Guillemin, E.P. Kanter, B. Krässig, D.W. Lindle, S.H. Southworth, R. Wehlitz, J. Baker, A. Hudson, M. Lotrakul, D. Rolles, W.C. Stolte, I.C. Tran, A. Wolska, S.W. Yu, M.Y. Amusia, K.T. Cheng, L.V. Chernysheva, W.R. Johnson, S.T. Manson, Dramatic nondipole effects in low-energy photoionization: Experimental and theoretical study of Xe $5s$, Phys. Rev. Lett. 91 (2003) 053002.
[21] E.W.B. Dias, H.S. Chakraborty, P.C. Deshmukh, S.T. Manson, O. Hemmers, P. Glans, D.L. Hansen, H. Wang, S.B. Whitfield, D.W. Lindle, R. Wehlitz, J.C. Levin, I.A. Sellin, R.C.C. Perera, Breakdown of the independent particle approximation in high-energy photoionization, Phys. Rev. Lett. 78 (1997) 4553.
[22] D.L. Hansen, O. Hemmers, H. Wang, D.W. Lindle, P. Focke, I.A. Sellin, C. Heske, H.S. Chakraborty, P.C. Deshmukh, S.T. Manson, Validity of the independent-particle approximation in X-ray photoemission: The exception, not the rule, Phys. Rev. A 60 (1999) R2641.
[23] R. Reininger, V. Saile, A soft X-ray grating monochromator for undulator radiation, Nucl. Instrum. Methods A 288 (1990) 343.
[24] C.U.S. Larsson, A. Beutler, O. Björneholm, F. Federmann, U. Hahn, A. Rieck, S. Verbin, T. Möller, First results from the high resolution XUV undulator beamline BW3 at HASYLAB, Nucl. Instrum. Methods A 337 (1994) 603.
[25] S. Ricz, A. Kövér, M. Jurvansuu, D. Varga, J. Molnár, S. Aksela, High-resolution photoelectron–auger-electron coincidence study for the $L_2 3 - M_2 3 M_2 3$ transitions of argon, Phys. Rev. A 65 (2002) 042707.
[26] R. Guillemin, O. Hemmers, D.W. Lindle, S.T. Manson, Experimental investigation of nondipole effects in photoemission at the advanced light source, Radiat. Phys. Chem. 73 (2005) 311.
[27] A. Derevianko, W.R. Johnson, K.T. Cheng, Non-dipole effects in photoelectron angular distributions for rare gas atoms, Data Nucl. Data Tables 73 (1999) 153.
[28] L. Gulyás, P.D. Fainstein, A. Salin, CDW-EIS theory of ionization by ion impact with Hartree–Fock description of the target, J. Phys. B 28 (1995) 245.
[29] J.W. Cooper, Photoelectron-angular-distribution parameters for rare-gas subshells, Phys. Rev. A 47 (1993) 1841.
[30] For a complete description of the atomic structure calculation based on Hartree Fock, see, R.D. Cowan, Theory of Atomic Spectra, University of California Press, Berkely, 1981;
The collisional excitation code is based on the method of Mann, J.B. Mann, At. Data Nucl. Data Tables 29 (1983) 407;
A description of the scaled hydrogenic ionization method can be found in, R.E.H. Clark, J. Abdallah Jr, J.B. Mann, Astrophys. J. 381 (1991) 597.
[31] A. Kramida, Cowan code: 50 years of growing impact on atomic physics, Atoms 2019 7 (2019) 1.
[32] E. Seres, J. Seres, S. Namba, J. Afa, C. Serrat, Attosecond sublevel beating and nonlinear dressing on the $3d$-to-$5p$ and $3p$-to-$5s$ core-transitions at 91.3 eV and 210.4 eV in krypton, Opt. Express 25 (2017) 31774.
[33] B. Krässig, E.P. Kanter, S.H. Southworth, R. Guillemin, O. Hemmers, D.W. Lindle, R. Wehlitz, N.L.S. Martin, Photoexcitation of a dipole-forbidden resonance in helium, Phys. Rev. Lett. 88 (2002).